Max-Planck-Institut
für Mathematik
in den Naturwissenschaften
Leipzig

Self-organized criticality in a mesoscopic model of excitatory-inhibitory neuronal populations by short-term and long-term synaptic plasticity

(revised version: April 2022)

by

Jürgen Jost and Masud Ehsani

Preprint no.: 14 2022

Self-organized criticality in a mesoscopic model of excitatory-inhibitory neuronal populations by short-term and long-term synaptic plasticity

Masud Ehsani[1*] and Jürgen Jost[1,2]

[1*] Max Planck Institute for Mathematics in Sciences, Inselstr.22, Leipzig, 04103, Saxony, Germany .
[2]Santa Fe Institute, 1399 Hyde Park Rd, Santa Fe, NM 87501, United States .

*Corresponding author(s). E-mail(s): masud.ehsani@mis.mpg.de;
Contributing authors: jjost@mis.mpg.de;

Abstract

In Ehsani and Jost (2022), we have shown that the dynamics of an interconnected population of excitatory and inhibitory spiking neurons wandering around a Bogdanov-Takens (BT) bifurcation point can generate the observed scale-free avalanches at the population level and the highly variable spike patterns of individual neurons. These characteristics match experimental findings for spontaneous intrinsic activity in the brain. In this paper, we address the mechanisms causing the system to get and remain near this BT point. We propose an effective stochastic neural field model which captures the dynamics of the mean-field model. We show how the network tunes itself through local long-term synaptic plasticity by STDP and short-term synaptic depression to be close to this bifurcation point. The mesoscopic model that we derive matches the directed percolation model at the absorbing state phase transition.

Keywords: Critical Brain Hypothesis, Bogdanov-Takens Bifurcation, Scale-free Avalanches, Self-organization , STDP , Short term depression

1 Introduction

Neural networks as complex dynamical systems with many degrees of freedom varying over different time scales can be seen as a self-tuning system that attains a dynamical regime where the system can carry out its task. On the other hand, spontaneous intrinsic activity of cortical neural assemblies in absence of any information processing task can be perceived as a substrate for the neural dynamics which can give us insights into the preferred dynamical regime and the goal of self-organization processes. Dynamic and functional characteristics of spontaneous activity are connected to the structural architecture of the brain as well as the ongoing self-organization process. Experimental findings on different temporal and spatial resolutions highlight the scale-free characteristic of spontaneous activity. When recorded by coarse-grained methods like EEG and MEG, spontaneous brain activity shows nested oscillations with a power spectrum that indicates scale-free properties, i.e. $P(f) \propto 1/f^{\beta}$(Linkenkaer-Hansen et al (2001); Miller et al (2009); Hardstone et al (2012)). Microelectrode recordings of smaller cortical regions show activity in the form of avalanches with power-law distributions of size and duration in different setups such as cultured slices of rat cortex (Beggs and Plenz (2003)), awake monkeys (Petermann et al (2009)), in cerebral cortex and hippocampus of anesthetized, asleep, and awake rats (Ribeiro et al (2010)) and visual cortex of anesthetized cat (Hahn et al (2010)).

One explanation for the scale-free characteristics is that cortical networks operate near a critical second-order phase transition (Chialvo (2004); Tagliazucchi and Chialvo (2013)). On one hand, close to the edge of an active-inactive phase transition, local populations of neurons in the cortex would be in an idle state ready for processing information, but at the same time away from overactivation. On the other hand, close to the phase transition, an order parameter, a macroscopic state different from the inactive state, comes into existence. The emergence of a macroscopic mode of activity acts as the coordinator of individual neurons which are enumerated in quantity and prone to various kinds of noise to produce a cooperative large-scale activity (Chialvo (2010). Macroscopic states of activity, in turn, enslave the individual neurons. These active states in the spontaneous mode in the absence of meaningful information processing tasks can be seen as either a random sequence of active neurons or activation of a sequence of already inscribed patterns of co-activity in the connectivity map. Mean-field models of neural dynamics can be used as the first step in the coarse-grained description of the neural network. Rate models can accurately describe neural networks in all-to-all or sparsely connected networks. The appropriateness of mean-field solutions for the all-to-all network in the limit of large size should be clear. On the other hand, in a sparsely connected network, correlations among the input to two different neurons, beyond the average population rate, are assumed to be negligible, and correspondingly also the magnitude of cross-correlation between spike trains of neurons is small. Therefore, in the population of neurons in low firing regimes

and in the sparsely connected network in which neurons fire with Poisson statistics but asynchronously, the total population rate dynamics can be modeled by a mean-field equation. The asynchronous state of population rate in the EI population can itself be oscillatory. In Brunel and Hakim (1999) and Brunel (2000), a sparsely connected network with synaptic delay between inhibitory feedback and the excitatory rate has been studied using a Fokker-Planck formalism for the evolution of the membrane voltage in the asynchronous state. Brunel and Hakim (2008) also studied fast global oscillations in neural networks operating at a low rate. The above-mentioned rate equations, also called Neural Mass Models, can be extended to the continuum limit. Continuum neural field models as nonlinear integrodifferential equations with the integral kernel representing the connectivity strength between different neural populations have been introduced by Wilson and Cowan (1972, 1973). Neural field models can show wave propagation in terms of a front solution in a bistable network (see Amari (1977); Ermentrout (1998)), propagating pulses in an excitable medium (see Pinto and Ermentrout (2001b)), and spatially localized oscillations and spiral waves in the oscillatory regime of a local EI population (Troy and Shusterman (2007)). They can also have localized bump solutions Pinto and Ermentrout (2001a) and spatially periodic patterns called Turing patterns (Ermentrout and Cowan (1979)). Weakly nonlinear analysis, singular perturbation methods, symmetric bifurcation theory, homogenization theory, and stochastic processes are the analytic tools for investigating these patterns of activity. (See Bressloff (2011), for a comprehensive review.)

Mean-field solutions can only exist in the limit of $N \to \infty$ and are based on neglecting correlations among neurons and finite-size effects. Stochastic neural networks have been proposed to account for fluctuations in the asynchronous state of firing and studying their correlations and finite-size effects in different studies (Ginzburg and Sompolinsky (1994); Meyer and van Vreeswijk (2002); Soula and Chow (2007); Touboul et al (2015)). These networks model microscopic neural dynamics as a Markov process based on the assumption that neural dynamics is Markovian. Truncation at the first moment of the mentioned Markov process is compatible with the mean-field equation. By truncation of the higher moments based on the assumption that pairwise correlations are of order $1/N$ and p-moments are of order $1/N^{p-1}$, we can derive closed-form equations for higher moments of activity of neurons or subpopulations of neurons. The main assumption is that in the asynchronous state auto-correlations are of order $1/N$. Bressloff (2000) utilized system size expansion of the master equation to systematically truncate the moment hierarchy based on the system size. Moreover, the stochastic version of the continuum neural field has been discussed in Buice and Cowan (2007) and Bressloff (2019).

In general, the mesoscopic description of dissipative systems in which the flow and fluctuation of energy are not based on the equilibrium fluctuations, such as general reaction-diffusion systems, is very complicated. The absence of detailed balance in microscopic dynamics and the fluctuation-dissipation theorem would make a straightforward phenomenological mesoscopic approach

like the Langevin dynamics for systems close to equilibrium impossible. However, for the non-equilibrium system which has a steady-state close to a critical point and shows generic scale invariance, an effective dynamical description in terms of a mesoscopic field equation is in general possible. In the critical state, the perturbations in the system spread in all length and time scales of the system with power-law distributions of size and duration.

In this case, we can write down the dynamics of the system out of equilibrium in terms of the microscopic master equation, like for interacting particle systems. Using the well-known coherent path integral procedure first introduced in the context of reaction-diffusion equations by Doi and Peliti (Doi (1976); Peliti (1985)) to form a non-Hermitian bosonic Hamiltonian and a continuum field representation, internal fluctuations are automatically taken into account. By using the perturbation approach and the renormalization group method, we can study the scale invariance and critical behavior of the model. Subsequently, the field theory representation in terms of a path integral over stochastic paths can be translated to the Langevin equation with an appropriate noise term using Janssen-Dedominicis functional representation.

Buice and Cowan used a coherent path formalism and the Doi-Peliti functional representation to translate the microscopic master equation to a path integral representation for activity fields (Buice and Cowan (2007)) . One advantage of their method is that the study of scale invariance at criticality in the functional representation is possible. They proposed that the stochastic neural field equation for the excitatory system at a critical point can be written in the form of Langevin's description of directed percolation. Benayoun et. al. proposed a stochastic model of spiking neurons which matches the Wilson-Cowan mean field in the limit of infinite system size that shows scale-free avalanches in the balanced state in which sum of excitation and inhibition is much larger than the net difference between them (Benayoun et al (2010)). Under symmetry condition on weights this makes the Jacobian to have negative eigenvalues close to zero in the balanced state. Cowan et al (2013) used the method of path integral representation in the stochastic model of spiking neurons supplemented by anti-Hebbian synaptic plasticity as the self-organizing mechanism. Their network possesses bistability close to the saddle-node bifurcation point which is the origin of the avalanche behavior in the system.

To tune the system at the critical point, many modeling approaches and adaptive mechanisms have been suggested during the decades of research on the critical brain hypothesis. A SOC model for a non-conservative neuronal model that attracted much attention is introduced by Levina et al (2009, 2007). In addition to self-organization by short-term depression in synapses which is also used in Peng and J. (2013) and di Santo et al (2018), self-organization by other control parameters like degree of connectivity or synaptic strength has been studied. Adaptive rewiring of asymmetric synaptic connections with fixed strength ($J_{ij} = \pm 1$) by the average input correlation was introduced in the spin models of neural networks (Bornholdt and Roehl (2003); Rybarsch and

Bornholdt (2014)). In these works, the authors have claimed that insertion and deletion of the links based on adaptive rewiring regulate the network toward criticality by tuning the branching ratio to unity.

In line with the methods used in those, Meisel and Gross (2009) introduced a self-organizing neural network by STDP. In Brochini et al (2016), self-organization in stochastic spiking neuron model by short term plasticity of the gain function instead of synaptic weights is introduced. Benayoun et al (2010) proposed a model composed of stochastic single neurons which shows avalanche dynamics in the regime of closely balanced input.

In Ehsani and Jost (2022), we showed that the Bogdanov-Takens bifurcation point of the mean-field equations for dynamics of an sparse homogenous excitatory and inhibitory population of spiking neurons with conductance-based synaptic currents is the operating point of the system producing the characteristic spontaneous activity in the form of scale-free avalanches. Here, we consider the self-tuning of the system at this critical point. The self-organizing parameter in our network is the balance of opposing forces resulting from the activities of inhibitory and excitatory populations, and the self-organizing mechanisms are long-term synaptic plasticity through the mechanism of Spike Timing Dependent Plasticity (STDP) and homeostatic short-term depression of the synapses. The former tunes the overall strength of excitatory and inhibitory pathways to be close to a balanced regime of these currents and the latter, which is based on the finite amount of resources in brain areas, acts as an adaptive mechanism that tunes micro populations of neurons subjected to fluctuating external inputs to attain the balance in a wider range of external input strengths. For analytical analysis of STDP on average weight connections, we use the inhomogenous Poisson neuron assumption that has been studied in Kistler and van Hemmen (2000) and Burkitt et al (2007). Under general conditions on inhibitory and excitatory STDP kernels, i.e. negative integral of the excitatory and positive integral of the inhibitory STDP kernels, learning results in a balanced internal state. This condition on kernels leads to stabilization of rates as also discussed in Kempter et al (2001). We use the model of Tsodyks and Markram (1997) for short-term depression of the excitatory synapses which has been studied vastly (see for example Kistler and van Hemmen (1999)).

Using the Poisson firing assumption, we propose a microscopic Markovian model which captures the internal fluctuations in the network due to the finite size and matches the macroscopic mean-field equation by coarse-graining. Near the critical point, a phenomenological mesoscopic model for excitatory and inhibitory fields of activity is possible due to the time scale separation of slowly changing variables and fast degrees of freedom. We will show that the mesoscopic model corresponding to the neural field model near the local Bogdanov-Takens bifurcation point matches the Langevin description of the directed percolation process. Tuning the system at the critical point can be achieved by coupling fast population dynamics with slow adaptive gain and synaptic weight dynamics, which make the system wander around the phase

transition point. Therefore, by introducing short-term and long-term synaptic plasticity, we have proposed a self-organized critical stochastic neural field model.

2 Materials and Methods

2.1 Neuron model

We use an integrate and fire neuron model in which the change in the membrane voltage of the neuron receiving time dependent synaptic current $i(t)$ follows

$$C\frac{dv(t)}{dt} = g_{Leak}(v_{Leak} - v(t)) + i(t) \tag{1}$$

for $v(t) < v_{th}$. When the membrane voltage reaches $v_{th} = -50mv$, the neuron spikes and immediately its membrane voltage resets to v_{rest} which is equal to $v_{Leak} = -65mv$.

In the following, we want to concentrate on a model with just one type of inhibitory and one type of excitatory synapses, which can be seen as the average effect of the two types of synapses. We can write the synaptic inhibitory and excitatory current as

$$i(t) = g_{inh}(t) * (V_{Rinh} - v(t)) + g_{exc}(t) * (V_{Rexc} - v(t)) \tag{2}$$

V_{Rinh} and V_{Rexc} are the reverse potentials of excitatory and inhibitory ion channels, and based on experimental studies we choose values of $-80mv$ and $0mv$ for them respectively. $g_{Inh}(t)$ and $g_{Exc}(t)$ are the conductances of inhibitory and excitatory ion channels. These conductances are changing by the inhibitory and excitatory input to the cell. Each spike of a presynaptic inhibitory or excitatory neuron j to a postsynaptic neuron k that is received by k at time t_0 will change the inhibitory or excitatory ion channel conductance of the postsynaptic neuron for $t > t_0$ according to :

$$\begin{aligned} g^k_{Inh}(t) &= w_{kj} * g_0^{inh} * exp(-\frac{t - t_0}{\tau_{syn}^{inh}}) \\ g^k_{Exc}(t) &= w_{kj} * g_0^{exc} * exp(-\frac{t - t_0}{\tau_{syn}^{exc}}) \end{aligned} \tag{3}$$

Here we assume that the rise time of synaptic conductances is very small compared to other time scales in the model and therefore, we modeled the synaptic current by a decay term with synaptic decay time constant τ_{syn} which we assume to be the same value of $5ms$ for both inhibitory and excitatory synapses.

2.2 Network architecture

In the remainder of this work, in the simulation, we consider a population of $N_{Exc} = 2 * 10^4$ and $N_{Inh} = 0.25 * N_{Exc}$ inhibitory spiking neurons with

conductance-based currents introduced in this section. Each excitatory neuron in the population is randomly connected to $k_{EE} = \frac{N_{Exc}}{100} = 200$ excitatory and $k_{EI} = \frac{k_{EE}}{4}$ inhibitory neurons and each inhibitory neuron is connected to $k_{IE} = k_{EE}$ and $k_{II} = \frac{k_{EE}}{4}$ excitatory and inhibitory neurons, respectively. The weights of excitatory synaptic connections are in a range that $10 - 20$ synchronous excitatory spikes suffice to depolarize the target neuron to the level of its firing threshold when it is initially at rest at the time of input arrival. Weights are being drawn from a log-normal probability density with low variance. Therefore, approximately $O(\sqrt{k_{EE}})$ spikes are adequate for firing. Assuming homogeneity in the population as we have discussed in the introduction we can build a mean-field equation for the excitatory and inhibitory population in this sparse network, assuming each neuron receives input with the same statistics.

2.3 Avalanche regime of activity as desired operating point of the system

In Ehsani and Jost (2022), we have investigated dynamics of excitatory and inhibitory (EI) sparsely connected populations of spiking leaky integrate neurons with conductance-based synapses. We have seen that close to the Bogdanov-Takens bifurcation point of the mean field equation, the output firing of the population is in the form of avalanches with scale free size and duration distribution. This matches the characteristics of low firing spontaneous activity in the cortex. By linearizing gain functions and excitatory and inhibitory nullclines, we approximated the location of the BT bifurcation point. This point in the control parameter phase space corresponds to the internal balance of excitation and inhibition and a slight excess of external excitatory input to the excitatory population. Due to the tight balance of average excitation and inhibition currents, the firing of the individual cells is fluctuation-driven. Around the BT point, the spiking of neurons is a Poisson process and the population average membrane potential of neurons is approximately at the middle of the operating interval $[V_{rest}, V_{th}]$. Moreover, the EI network is close to both oscillatory and active-inactive phase transition regimes.

At equilibrium, population rates satisfy a system of fixed point equations of the form :

$$\begin{aligned} \rho_I &= g^I(\rho_I, c_{EI}\rho_E + c_{II}\rho_I + d\rho^I_{Ext}) - z_0 \\ \rho_E &= g^E(\rho_I, c_{EE}\rho_E + c_{EI}\rho_I + d\rho^E_{Ext}) - z_0 \end{aligned} \tag{4}$$

where $c_{xy} = ck_{xy}w_{xy}(V_{R_y} - \langle V_x \rangle)$. k_{xy} is the average number of synaptic connections between neurons of population y to neurons in population x with average strength of w_{xy}. z_0 is a constant that depends on V_{rest}, V_{th}, the maximal rates and the standard deviation of the input. V_{R_y} is the reverse potential

level of a neuron of type y and $\langle V_x \rangle$ is the average potential level of neurons in population x that can be written in fluctuation driven the firing regime as :

$$< V_x >= \frac{g_L V_L + g^0_{exc} w_{xE} \rho_E \tau V_{Rexc} + g^0_{inh} w_{xI} \rho_I \tau V_{Rinh}}{g_L + g^0_{exc} w_{xE} \rho_E \tau + g^0_{inh} w_{xI} \rho_I \tau} \tag{5}$$

τ is the synaptic current decay time constant, g_L , g_{exc} and g_{inh} are the baseline conductances of leaky, excitatory and inhibitory ion gates, respectively. We took w_{EE} and ρ^E_{Ext} as control parameters and analyzed solutions to the Eq.4. By substituting nonlinear gain functions with their corresponding linearization in the Poisson firing regime, we showed that the low BT point is located close to the matching condition for the y-intercept and the slopes of the linearized nullclines, which are written as:

$$\begin{aligned} c^*_{EE} &= \frac{c_{EI} c_{EI}}{c_{II}} \\ \rho^{E^*}_{Ext} &= \frac{c^*_{EE}}{c_{IE}} (\rho^I_{Ext} - d) + d \end{aligned} \tag{6}$$

where d is a constant equal to $\frac{g_L (V_{rest} - V_{th})}{\tau * g^0_{exc} * (V_{th} - V_{R_{exc}})}$.

3 Results

3.1 Long term synaptic plasticity by STDP tunes synaptic weights close to the balanced state

A typical neuron in the cortex has $10^3 - 10^4$ synaptic connections with 80% of them of excitatory type and 20% of inhibitory type. On the other hand, even in the resting state, neurons on average have a non-zero firing rate with an average rate of $1Hz$ and their spike trains are very noisy with exponential interspike interval distribution indicating that the spiking of individual neurons is a Poisson point process. Yet another experimental fact about synaptic strength between neurons states is that usually, $10 - 20$ presynaptic synchronous spikes suffice to bring a typical neuron to the firing threshold. If we take $\tau_m = 20ms$ as the membrane potential decay time constant, then during this time window a typical neuron receives $20 - 200$ excitatory spikes, which are enough for the neuron to periodically spike at a very high rate. To avoid this, the inhibitory input in this time window should largely cancel the excitatory current. Therefore, for the average currents to maintain the average membrane potential below the threshold in order to avoid a high firing state and produce high variability in the spike trains, inhibitory and excitatory currents should be balanced. Dynamical balance of excitation and inhibition ensures a low level of activity, i.e., an asynchronous firing state. In the following, we present a synaptic plasticity rule which tunes the average synaptic weights to the balanced state. We will analyze and simulate a network in which neurons

will adapt their connections according to the Spike-timing dependent plasticity (STDP) paradigm (Gerstner et al (1996)), which provides a foundation for temporal coding. We derive an equation for the evolution of the average and the variance of weights between excitatory and inhibitory neurons during the plasticity period. In STDP, the weight of a connection is modified depending on the time interval between pairs of pre- and post-synaptic spikes. For every pair, the weight of the synapse changes according to the equations

$$\Delta w(\Delta t) = \begin{cases} f_+(w)K_+(\Delta t) & \text{if } \Delta t \geq 0 \\ -f_-(w)K_-(\Delta t) & \text{if } \Delta t < 0 \end{cases} \tag{7}$$

where $\Delta t = t_{post} - t_{pre}$ is the time difference between the postsynaptic spike and the presynaptic one. The functions f_+ and f_- model the dependence of the weight change on the current value of the synaptic weights. K_+ and K_-, called STDP kernels, usually are decaying functions of time which reflects the fact that closer pre- and post-synaptic spikes generate stronger weight changes. Usually, we model the kernels by a single exponential such as $K_+ = A_+ e^{-\frac{|\Delta t|}{\tau_{s+}}}$ and $K_- = A_- e^{-\frac{|\Delta t|}{\tau_{s-}}}$. As it is evident from equation (7), when the postsynaptic neuron fires after the presynaptic neuron, the strength of the connection increases and it decreases for the opposite temporal order. We assume the same type of the STDP rule for both inhibitory and excitatory connections although with different kernels. In the following, we suppose that the dependence of STDP on the synaptic weight is negligible and therefore replace the functions f_+ and f_- by a constant which is then absorbed into the kernels. In this case, we have to assume a saturation level for the maximum strength of the synapses, w^E_{max} and w^I_{max}.

STDP changes synaptic weights on a very slow time scale compared to firing dynamics of the neurons, therefore, during a time period of $[t, t + \Delta t]$ where Δt is long in comparison with the inter-spike time interval but small enough that the change in the weight w_{ij} of the synapse from neuron j to neuron i is infinitesimal, we can write:

$$\begin{aligned} \Delta w_{ij} = &\int_t^{t+\Delta t} \int_0^\infty S_j(s) S_i(s+\delta) f_+(w_{ij}) K_+(\delta) d\delta ds \\ &+ \int_t^{t+\Delta t} \int_0^\infty S_i(s) S_j(s-\delta) f_-(w_{ij}) K_-(\delta) d\delta ds \end{aligned} \tag{8}$$

where $S_i(t)$ and $S_j(t)$ are the spike trains of the presynaptic and the postsynaptic neurons. Assuming that during this period, the firing rate of the output neuron is constant on average and there exist many pre- and post-synaptic spikes, we can write the mean change in the incoming synaptic weights to the

neuron i as,

$$\frac{\langle \Delta w_{ij} \rangle_j}{\Delta T} = \int_0^\infty \langle S_j(s) S_i(s+\delta) \rangle_j K_+(\delta) d\delta - \int_0^\infty \langle S_j(s) S_i(s-\delta) \rangle_j K_-(\delta) d\delta \quad (9)$$

We want to investigate the evolution of the synaptic weights in the EI population in an asynchronous irregular state. Therefore, we assume that in the regime of the spontaneous activity neurons are firing as a Poisson process. Moreover, to estimate the cross-correlation of the pre- and the post-synaptic spike train we argue that the excitatory input to the cell has a positive correlation with preceding spikes in the target neuron. The magnitude of this excess correlation depends on the weight of the synapse and it is restricted to the time window before the firing of the postsynaptic neurons. With this in mind, we use the following approximation introduced in Câteau and Fukai (2003) and van Rossum et al (2000) for the cross-correlations of spike trains to account for the causal contributions of presynaptic spikes to the postsynaptic ones of a synapse with the strength w_i:

$$\begin{aligned} \langle S^E_{pre}(s) S^E_{post}(s+\delta) \rangle &= \rho^E_{pre} \rho_{post} + \rho^E_{pre} w_i (V_{Rexc} - V_i) \gamma^E(\delta) \\ \langle S^I_{pre}(s) S^E_{post}(s+\delta) \rangle &= \rho^I_{pre} \rho_{post} - \rho^I_{pre} w_i (V_i - V_{Rinh}) \gamma^I(\delta) \end{aligned} \quad (10)$$

Here V_i is the voltage level of the postsynaptic neuron. As the second terms in both equations encode the excess correlation (anticorrelation) of the presynaptic excitatory(inhibitory) input preceding the firing at the postsynaptic neuron, we set $\gamma^I(\delta) = \gamma^E(\delta) = 0$ for $\delta < 0$. For positive values of δ, this function which is independent of the rates and the weights of the synapses, encodes the causal effect of the presynaptic spike which arrives δ units of time before firing of the postsynaptic neuron. Therefore, it is a decaying function of δ. Moreover, we have assumed the dependence on the weight of the synapse to be of a linear form, which is a good approximation in the regime of small synaptic weights. Inserting the above approximation and labeling the STDP kernels of EE and IE synapses as K^E and the STDP kernels of II and EI synapses as K^I, we can write the evolution of the average excitatory and inhibitory synaptic strength to the neuron i as

$$\begin{aligned} \frac{d\langle w^E_{ij} \rangle}{dt} &= \langle \rho^E_j \rangle \rho_i (\overline{K}^E_+ - \overline{K}^E_-) + \langle \rho^E_j \rangle \langle w^E_{ij} \rangle (V_{Rexc} - \langle V_i \rangle) \overline{K^E_+ \gamma^E} \\ \frac{d\langle w^I_{ik} \rangle}{dt} &= \langle \rho^I_k \rangle \rho_i (\overline{K}^I_+ - \overline{K}^I_-) - \langle \rho^I_k \rangle \langle w^I_{ik} \rangle (\langle V_i \rangle - V_{Rinh}) \overline{K^I_+ \gamma^I} \end{aligned} \quad (11)$$

Here, bars denote integrals of the kernels on the positive or negative real lines. In the population of sparsely connected and sufficiently homogeneous neurons, in terms of the number of connections of each neuron, and the regime of asynchronous homogeneous firing, i.e., when all the neurons fire with the same average rate but with a random phase of firing between them, the average weights evolve as

$$\begin{aligned} \frac{dw_{EE}}{dt} &= \rho^2_E \hat{K^E} + \rho_E w_{EE} (V_{Rexc} - \langle V^E \rangle) \overline{K^E_+ \gamma^E} \\ \frac{dw_{EI}}{dt} &= \rho_E \rho_I \hat{K^I} - \rho_I w_{EI} (\langle V^E \rangle - V_{Rinh}) \overline{K^I_+ \gamma^I} \end{aligned}$$

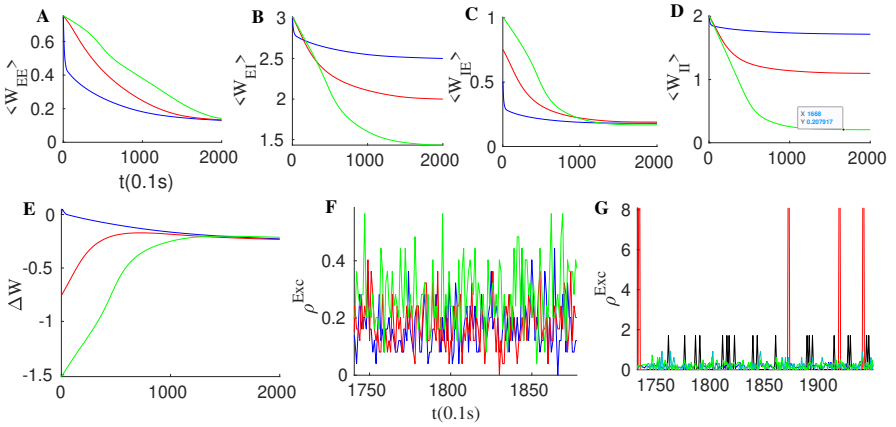

Fig. 1: Effect of synaptic plasticity on network with three different initial weight configurations when external excitatory input to both excitatory and inhibitory populations are of same magnitude ρ_{Ext}= 150Hz . (A-D) Evolution of average synaptic weights by STDP. (E) Change in the balance condition by STDP. Slopes of the Exc. and the Inh. nullclines approach each other under STDP in all three configurations. (F) The final state of the average neuron firing rates for these three networks lies below 1Hz. (G) Network activity for different clusters of neurons with different overall average inward synaptic weights. STDP results in clusters with different overall connectivity strengths and correspondingly different average rates.

$$\begin{aligned}\frac{dw_{IE}}{dt} &= \rho_E \rho_I \hat{K^E} + \rho_E w_{IE}(V_{Rexc} - \langle V^I \rangle)\overline{K_+^E \gamma^E} \\ \frac{dw_{II}}{dt} &= \rho_I^2 \hat{K^I} - \rho_I w_{II}(\langle V^I \rangle - V_{Rinh})\overline{K_+^I \gamma^I}\end{aligned} \tag{12}$$

From the above equations, it is straightforward to see when $\hat{K^E} := \overline{K}_+^E - \overline{K}_-^E < 0$ and $\bar{K^I} := \overline{K}_+^I - \overline{K}_-^I > 0$, the stationary solutions satisfy :

$$\frac{c_{EI}^{st}}{c_{EE}^{st}} = \frac{\hat{K^I}\overline{K_+^E \gamma^E}}{\hat{K^E}\overline{K_+^I \gamma^I}} = \frac{c_{II}^{st}}{c_{IE}^{st}} \tag{13}$$

We take the proportion of inhibitory synapses to excitatory synapses to be equal for both excitatory and inhibitory neurons, i.e. $\frac{k_{EI}}{k_{EE}} = \frac{k_{II}}{k_{IE}}$. The above condition brings the slopes of the excitatory and the inhibitory nullclines close to each other (Equation (6)) leading to intersection in the semi-linear regime and proportionality of excitation and inhibition:

$$\frac{\rho_I^{st}}{\rho_E^{st}} \approx \frac{c_{EE}}{c_{EI}} \tag{14}$$

As the system lies around the BT point, synaptic plasticity has a strong effect when neurons are in a higher (here the linear) firing regime. At this state, rates vary co-linearly according to the above equation. On the other hand, synaptic plasticity rules for w_{II} and w_{EI}, i.e., the second and fourth lines in equation (13), lead to a relation for stationary weights in the form of $\frac{c_{II}}{c_{EI}} = \frac{k_{II}\rho_I^{st}}{k_{EI}\rho_E^{st}}$. Comparing these last two equations, we arrive at $k_{II}c_{EE}^{st} = k_{EI}c_{II}^{st}$. Assuming $k_{II} = k_{EI}$, the mentioned relation adjusts the trace of the Jacobian at the fixed point in the linear section to be near zero. Therefore, the plasticity rule and the dynamics of the near-linear regime stabilizes the system near the BT point. Figure (1) shows that STDP brings the network of EI populations to the avalanche regime. As STDP leads to an increase in the variance of the weight distribution, some groups of neurons become highly connected to each other while other groups show less overall connectivity strength. These groups of neurons will have different average rates as can be seen in Figure 1G.

3.2 Short-term plasticity tunes the network in a wide range of external input

In the following, firstly, we will discuss the adaptive role of short-term synaptic plasticity in bringing the network of the EI population to the avalanche regime. Afterward, we will discuss how internal or external noise close to the BT point can also cause the switch between the quiescent (Down) and the low firing (Up) states. We will discuss that the Up-Down state transition by short-term depression can be achieved either through a switch between bi-stable states or by bringing the system close to the BT point by dampening the overall excitation. We use the model of Tsodyks and Markram (1997) for short-term depression of the excitatory synapses reduces the outgoing synaptic efficacy of excitatory synapses to an excitatory neuron in case of a high rate of presynaptic activity. To model the STP effect, we assume that the effective utility of the excitatory synapses of neuron j to the other neurons is proportional to the fraction of the available synaptic resources u. Decrease of neurotransmitters at the synapses and depression in release probability due to consecutive uses of neurotransmitters in previous spikes of the presynaptic neuron are the sources of STP. We assume by each spike of a presynaptic neuron, u is reduced by the factor qu and then recovers with time constant τ_{STP} which is of order $100ms$ to a few seconds. Therefore, synaptic efficacy of the postsynaptic synapse of neuron j evolves as:

$$\frac{du_j}{dt} = \frac{1}{\tau_{STP}}(1 - u_j) - qu_j \sum_k \delta(t - t_k^j) \tag{15}$$

Here, we just consider the short-term plasticity of synapses between excitatory neurons. This type of plasticity might occur in other types of synapses as well, but we will not discuss this here. Because there exist numerous input synapses and we have assumed homogeneous connectivity, each neuron senses

a large sample of the network activity and is connected with an overall average weight with a small variance to the excitatory neuron pool. Based on these assumptions and structural homogeneity, we can write down the dynamic of the average synaptic weights to the neuron i in the state of the network with excitatory population firing rate of magnitude ρ_E as :

$$\frac{dw_{EE}}{dt} = \frac{w^0_{EE} - w_{EE}(t)}{\tau_{STP}} - w_{EE}(t) q \rho_E(t) \tag{16}$$

The rate equations for the EI population are of the form:

$$\begin{aligned} \frac{d\rho_E}{dt} &= -\frac{1}{\tau_m}(\rho_E(t) - f(\rho_E(t), \rho_I(t), w_{EE}(t))) \\ \frac{d\rho_I}{dt} &= -\frac{1}{\tau_m}(\rho_I(t) - g(\rho_E(t), \rho_I(t))) \end{aligned} \tag{17}$$

Taking the time scale of short term plasticity to be much larger than the EI-network activity decay time constant, i.e. $\tau_{STP} >> \tau_m$, we can rewrite the dynamic in terms of fast, d/dt^f, and slow time, d/dt^s, evolution. Here, $t_f = t/\tau_m$ and $t_s = t/\tau_{STP}$. Defining $\mu = t_s/t_f$ and $\rho = \begin{pmatrix} \rho^E \\ \rho^I \end{pmatrix}$, we arrive at

$$\begin{aligned} \frac{d\rho}{dt^f} &= -(\rho - f(\rho, w_{EE})) \\ \frac{dw_{EE}}{dt^f} &= \mu(w^0_{EE} - w_{EE}) - q\tau_m w_{EE} \rho^E \end{aligned} \tag{18}$$

This set of equations can have a stable fixed point or an oscillatory behavior. The average synaptic efficacy in the stationary state with the average excitatory rate ρ^*_E is:

$$\langle w_{EE} \rangle_{St} = \frac{w^0_{EE}}{1 + \tau q \rho^*_E} \tag{19}$$

In case that there exists a fixed point or a stable limit cycle solution around this point in the $(\rho_E, \rho_I, \langle W_{EE} \rangle_{st})$ phase space, the system might settle down at this solution (Fig.2A). The dynamics of the EI population near this region (with the slow-fast assumption) can be written as

$$\begin{aligned} \rho^{st}_E &= f(k_{EE}\rho^{st}_E, k_{EI}\rho^{st}_I, \lambda^{Ex}_E, \lambda^{Ex}_I, \frac{w^0_{EE}}{1 + \tau q \langle \rho^{st} \rangle}) \\ \rho^{st}_I &= g(k_{EI}\rho^{st}_E, k_{II}\rho^{st}_I, \lambda^{Ex}_E, \lambda^{Ex}_I) \end{aligned} \tag{20}$$

This mechanism is effective to bring the system close to the BT point. Short synaptic plasticity is a method of gain control that can bring the system from a wide range of input and initial states to the low activity background state. In Fig.3, we consider a system that is already tuned by STDP to the balanced state of weights (Eq. 13) receiving various rates of external excitatory input

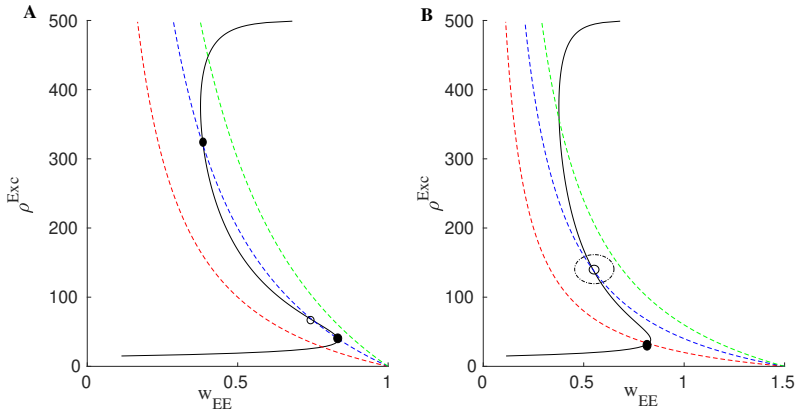

Fig. 2: Output excitatory rates as a function of W_{EE} and the corresponding graphs for the average synaptic efficacy $\langle W_{EE} \rangle_{St}$ at three values of q (dashed red curve belongs to the largest and the dashed green curve is for the lowest value). Based on the value of W^0_{EE}, two different scenarios can occur. In (A) by decreasing q, through a saddle-node bifurcation stable and unstable fixed points appear at low and high values of the rates. In (B), with higher W^0_{EE}, by decreasing q after the Hopf bifurcation of the low firing rate fixed point, an oscillatory solution for (u, ρ_{out}) emerges.

to the excitatory population. In all cases, the system is initially away from the BT point. Without STP, the system shows a high firing rate oscillatory activity with an average rate of around $300Hz$. STP brings all of them closer to the avalanche regime. The average synaptic efficacy $\langle u \rangle$ in these cases does not oscillate significantly. As the system resides closer to the low firing regime through lowering the effective synaptic strength of Exc.-Exc. connections by STP, on a longer time scale STDP transforms the combination of weights to move the system to the avalanche regime by aligning the slopes of linearized nullclines.

When the external input rate is tuned very close to the BT point, where the quiescent fixed point and a low firing weakly (un)stable point lie close to each other, we see asynchronous avalanches of highly variable sizes (see Fig. 4A and Fig.8A). Without STP, we observe higher rates and less variable quiescent (Down) state time intervals (Fig.4B). Finite-size fluctuations kick the system out of the quiescent fixed point while STP plus fluctuations at the low rate fixed point drive the system back to the quiescent state. Average membrane potential as well as single neuron potentials in this case shows a transition between two levels (see Fig.4B_2).

Fig.5A shows excitatory and inhibitory stationary rates of the EI population subject to external rates in the range [200-500]Hz. As can be seen, STP leads to low firing rate states and prevents overactivation. Fig.4C shows avalanche size distribution in a log-log plot for avalanches as in Fig.4A. The

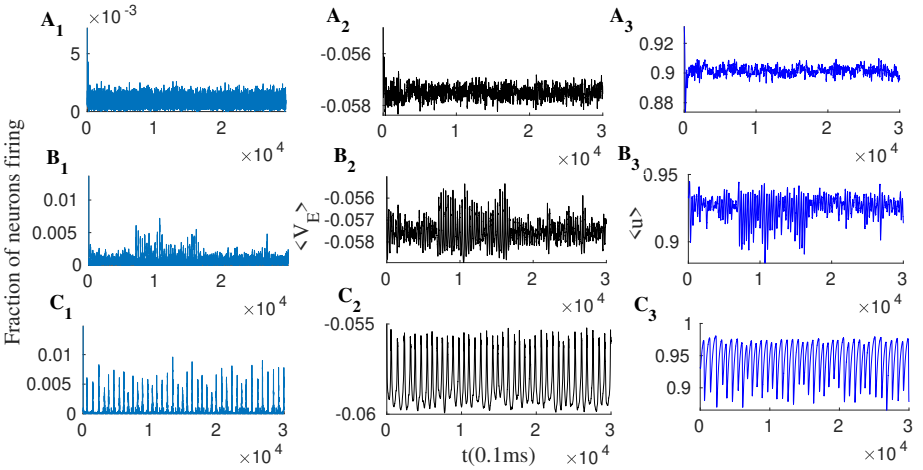

Fig. 3: EI population with short term plasticity. $W_{EI} = 1.5, W_{II} = 2, W_{IE} = 0.75, W^0_{EE} = 0.54$, ρ^{inh}_{Ext}= 150Hz and $\rho^{exc}_{Ext} = [380, 280, 240]$Hz. STP parameters are $q = 0.3$, $\tau_{STP} = 10 * \tau_{syn}$. The top panel is the system with the highest external input rate and the bottom panel is the one with the lowest. Left plots show the excitatory population rates, middle plots the population average membrane potential and right plots the average excitatory synaptic efficacy $\langle u \rangle$.

slope of the linear regression line is very close to -1.5. The branching ratio for the final state of the system is shown in Fig.5B. For $\rho_{Ext} = 230Hz$, the branching ratio is slightly less than one which is in agreement with our prediction in the avalanche regime. Moreover, Fig.6 shows final output rates in the case of a stable fixed point for u for three different values of the external excitatory rates and W^0_{EE}.

Another way that STP can cause a switch between two distinct firing states is in the EI population which possesses bi-stability. In this case, change of u can make each of the bi-stable nodes unstable while the system resides near them. Decrease of u in the up-state makes the up-state fixed point unstable at some value of $u(t)$ (and accordingly w_{EE}). Therefore, the system will jump to the remaining stable fixed point in a low or quiescent state. In the very low firing regime (the quiescent state), u will recover to its asymptotic value, and the average synaptic weight increases towards w^0_{EE}. If the quiescent state is unstable when u approaches its maximum value, we observe a transition to the high state. Moreover, if the volume of the basin of attraction of the quiescent fixed point is small, external and internal noise can also induce the transition to the high rate fixed point and the quiescent fixed point need not become unstable at w^0_{EE}. For high values of u, the up-state fixed point is the stable point of the fast system but an unstable point of the slow one. Therefore, following the slow path up-state loses stability and the fast system remains with only a stable low fixed point. The trajectory of the slow u is oscillatory in

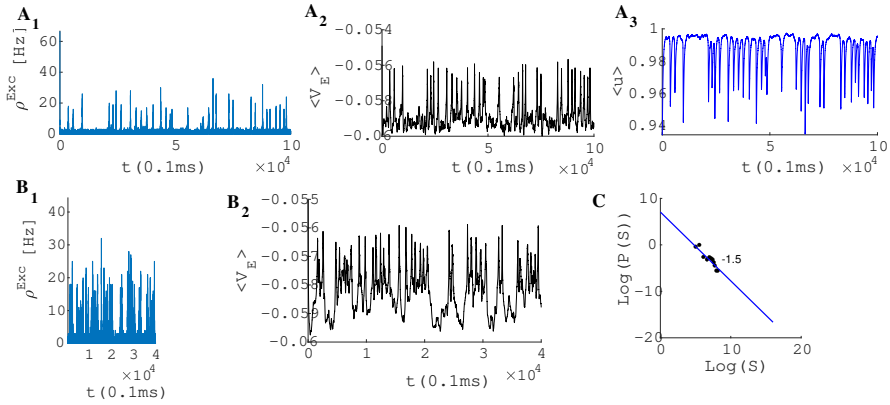

Fig. 4: (A)System with the same parameters values as in Fig.3 except that here $\rho_{Ext}^{exc} = 230Hz$. (B) EI population with same parameters as in Fig.4A but without STP. (C) Avalanche size distribution in a log-log plot for the network in Fig.4A.

this case. Fig.7 shows both ways that STP can produce synchronous avalanche behavior in the system. When $W_{EE} = w^0$, the system is close to the constraints on the alignment of the semi-linear segments of the EI-nullclines which results in the presence of a high firing state as a unique fixed point of the system. In the high input rate case, $\rho_{Ext} = 400Hz$, corresponding to Fig.7A and the nullcline diagram of Fig.8C, due to STP, the system moves from a high state of activity to a limit cycle solution at lower firing rates. This final state is shown in Fig.7A and nullcline arrangements in this state are depicted in Fig.8B. Here, there is an unstable source in the linear branch sector which is surrounded by a limit cycle. Moreover, oscillations in $\langle u \rangle$ have a low amplitude because of the temporal averaging. On the other hand, the two bottom panels in Fig.7 are related to the situation of a switch between the high fixed point and the quiescent node. As shown in nullcline graphs in Fig.8C, at high synaptic efficacy the high firing state is the only stable fixed point, however, a high firing rate leads to a fast decline of the synaptic efficacy which brings the system to the state with the nullcline map of Fig.8D which has a stable quiescent fixed point. The final state activity, in this case, is composed of avalanches with a high rate of firing in a short time window. Decreasing the q factor can result in a longer up-state period. Also, $\langle u \rangle$ oscillates between two limits in these cases.

In this particular case, necessary conditions for up to down transitions are:

$$\begin{aligned} k_{EE} W_{EE}^0 &> k_{EI} W_{EI} \\ k_{EE} \frac{w_{EE}^0}{1 + \tau q \rho^H} &< k_{EI} W_{EI} \end{aligned} \tag{21}$$

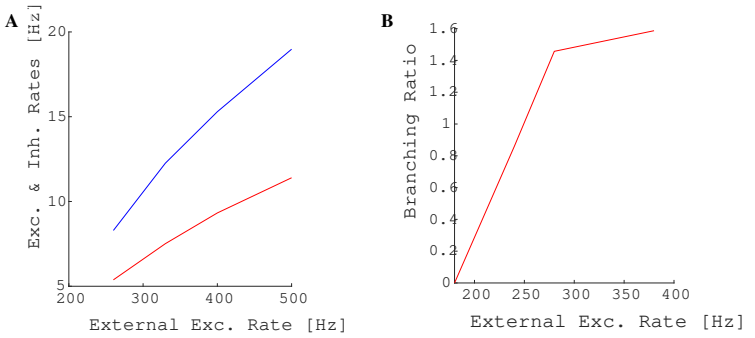

Fig. 5: (A) The final excitatory (red) and inhibitory (blue) output rates for the system in Fig.3 and Fig.4A . STP works as a gain control mechanism. (B) The branching ratio in the network states shown in Fig.3 and Fig.4A is defined as the average number of post-synaptic neurons of a single presynaptic neuron which set to fire by receiving the presynaptic input spike. Higher external rates set more neurons close to the threshold and thus the branching factor increases. When the inflection point of the steady membrane potential distribution passes the membrane threshold in the steady-state firing rate regime this increment rate slows down leading to the concavity of the branching factor curve.

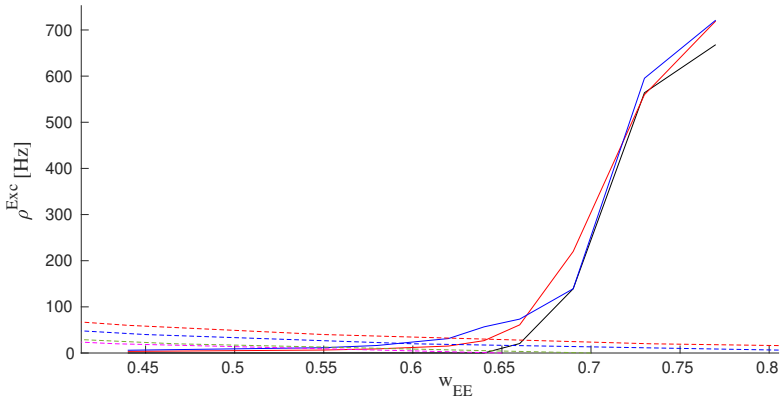

Fig. 6: Solid curves are the output rates for three different external input strengths vs. W_{EE}: Blue ($400Hz$), red ($310Hz$), and black ($220Hz$). Dashed curves show average stationary synaptic weight, $\langle W_{EE} \rangle$, in the network with STP with different maximum synaptic efficacies: W^0_{EE} =1.3 (red) , 0.9 (blue), 0.7 (green), and 0.65 (magenta). Intersections of the dashed and the solid curves are the fixed points of the EI network with STP for the corresponding control parameters. These fixed points are located in the low firing rate regime close to the avalanche region.

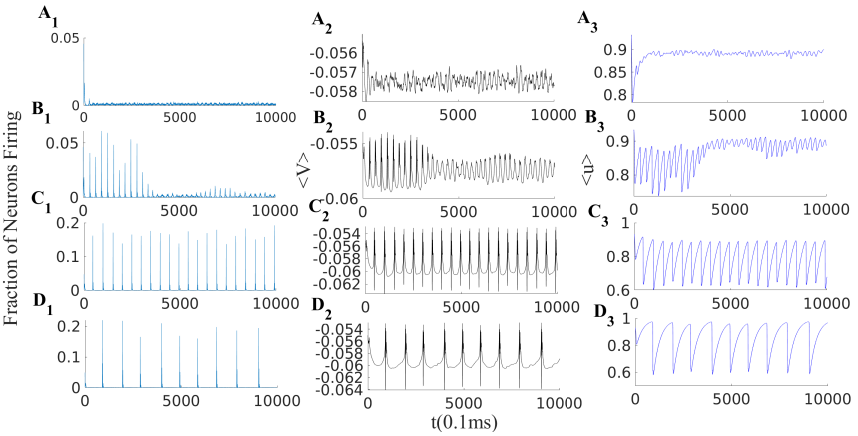

Fig. 7: EI population with short term plasticity. Network parmeters are : $W_{EI} = 2, W_{II} = 2, W_{IE} = 0.75$, $W^0_{EE} = 0.74$, ρ^{inh}_{Ext}= 150 Hz, ρ^{exc}_{Ext} =[400 ,330 , 270, 225] Hz and STP parameters are: $q = 0.4$, $\tau_{STP} = 10 * \tau_{syn}$. Left plots: excitatory rates; middle plots: average membrane potential; right plots: average synaptic efficacy $\langle u \rangle$.

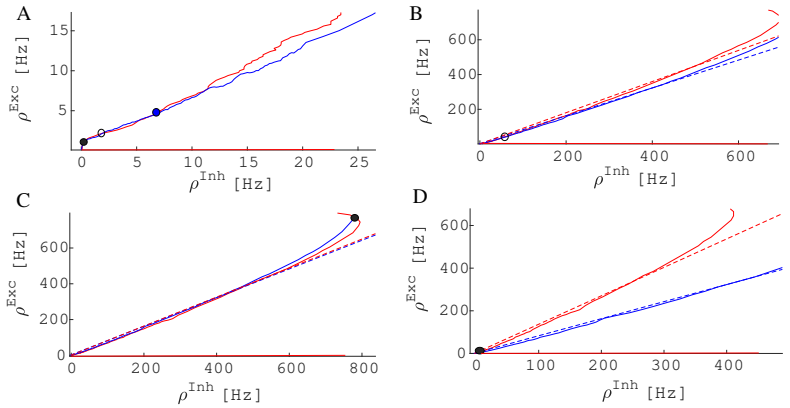

Fig. 8: Excitatory (red) and inhibitory (blue) nullclines, i.e solutions to Eq.4) for excitatory and inhibitory rate, respectively. Dashed lines are the linearized nullcline approximation with slopes of $k\frac{c_{EI}}{c_{EE}}$ (Exc.) and $k\frac{c_{II}}{c_{IE}}$ (Inh.) where k is a constant. STDP brings these slopes close to eachother (Eq. 13. (A) Nullclines at the Avalanche regime: The volume of the basin of attraction of the stable quiescent state is small and a weakly stable or unstable fixed point at the intersection in the semi-linear regime of nullclines is close to the origin. (B) System with only a saddle fixed point with a limit cycle solution with medium firing rates. (C) System with only a high firing fixed point. (D) System with only a stable quiescent state fixed point.

The first condition means that the slope of the excitatory nullcline is smaller than the inhibitory one, which indicates a stable high firing fixed point. The second condition states that at this high firing state the stationary weight is not accessible before a stability loss. The slope of nullclines increases by the decrease of effective W_{EE} which causes the high state to lose stability either through a Hopf or a saddle-node bifurcation.

Finally, the plots in Fig.7B depicts the case where STP brings the system close to the BT point that shows low to medium size avalanches with higher variability. In summary, transition from a quiescent state to a high firing state can be of two distinct types. One way is that by increasing W_{EE}, the LF fixed point and the unstable saddle move toward each other and in this way the basin of attraction of the LF fixed point shrinks and noise can initiate the escape from this fixed point to the high firing state. The other possibility is that a fixed point losses stability through a Hopf bifurcation either before or after the emergence of a saddle-node in the middle branch.

3.3 Avalanches and Turing instability in the interconnected network of EI populations

The model of Wilson and Cowan for the dynamics of the spatio-temporal mean fields of the excitatory and the inhibitory population rates, $E(x,t)$ and $I(x,t)$, in a 2D model of the cortex was introduced in the '70s. In this model at each point x, $E(x,t)$ is the density of the active neurons at time t in a sphere of radius Γ around x. Take a as the average distance between a neuron and its neighbors and ξ as the correlation length of the activity of neurons. Selecting $a << \Gamma < \xi$ guarantees that $E(x,t)$ is well defined and the number of neurons in each block is large enough to take the limit w.r.t. the size of the local population. $E(x,t)$ is defined as :

$$E(x,t) = \lim_{t\to 0} \lim_{N\to\infty} \frac{n_{active}(x, t+dt)}{N} \tag{22}$$

Where $n_{active}(x,t)$ is the number of active neurons in the time window $[t, t+dt]$ and N is the total number of neurons. Considering a high density of neurons, we assume that fluctuations in the number of the active neurons around this mean value are negligible. Furthermore, to derive the dynamics of this field we have to write down the input-output relation for each population of neurons at position x. In the mean-field approximation, we assume that each neuron receives the same input, which implies that each neuron is connected to all other neurons, and the weights of connections depend only on the distance $x - x'$ between two neurons. This can be a valid approximation if the connections between adjacent neurons are dense and the heterogeneity in the network structure is minimal. Now, assuming that neurons in each population relax to the non-active state in the absence of input with relaxation constant τ, one can consider

the following general equation for the activity field $E(x,t)$:

$$\tau \frac{dE(x,t)}{dt} = -E(x,t) + (k_e - r_e E(x,t)) * S_e(i_E(x,t)) \tag{23}$$

$i_E(x,t)$ is the input to the excitatory population at x at time t which consists of both inhibitory and excitatory currents from both the self-activity of neurons in the population and other neurons in the adjacent population. S_e is a nonlinear input-output function that in general depends on the response of the individual neurons, the distribution of the membrane voltage, and the heterogeneity in weights. In the following, like in Landau-Ginzburg modeling of a phase transition, we will assume that the fields $E(x,t)$ and $I(x,t)$ are very small so we can perform an expansion as a power series. Furthermore, since these are average fields, we assume that they vary slowly and smoothly in space, therefore, we neglect fast fluctuations and write down a phenomenological model for the current to the excitatory population as

$$\begin{aligned}
i_E(x,t) =& \int_V [E(x',t) w_{EE}(\text{x'-x}) + I(x',t) w_{EI}(\text{x'-x})] dV + i_E^{ext} \\
=& E(x,t) \int w_{EE} dV + \nabla E(x,t) \int (x'-x) w_{EE}(\text{x'-x}) dV \\
&+ \frac{1}{2} \int (x'-x) H_E(x) (x'-x) w_{EE}(\text{x'-x}) dV \\
&+ I(x,t) \int w_{EI} dV + \nabla I(x,t) \int (x'-x) w_{EI}(\text{x'-x}) dV \\
&+ \frac{1}{2} \int (x'-x) H_I(x) (x'-x) w_{EI}(\text{x'-x}) dV + i_E^{ext} \\
=& 2\pi E(x,t) \int r w_{EE}(r) dr + 2\pi I(x,t) \int r w_{EI}(r) dr \\
&+ \pi \nabla^2 E \int r^3 w_{EE}(r) dr + \pi \nabla^2 I \int r^3 w_{EI}(r) dr + i_E^{ext} \\
&+ \text{ higher order terms}
\end{aligned} \tag{24}$$

We can expand S^E around $I_0^e = 2\pi E(x,t)\overline{r w_{EE}} + 2\pi I(x,t)\overline{r w_{EI}} + i_E^{ext}$ and write :

$$\tau \frac{\partial E(x,t)}{\partial t} = -E(x,t) + (k_e - r_e E(x,t))[S^E(I_0^e) + \pi S^{E'}_{|I_0^E}(\nabla^2 E \langle r^3 w_{EE} \rangle + \nabla^2 I \langle r^3 w_{EI} \rangle)] \tag{25}$$

The same equation holds for the inhibitory field by expanding S^I around $I_0^i = 2\pi E(x,t)\overline{rw_{IE}} + 2\pi I(x,t)\overline{rw_{II}} + i_I^{ext}$:

$$\tau\frac{\partial I(x,t)}{\partial t} = -I(x,t) + (k_i - r_i I(x,t))[S^I(I_0^i) + \pi S^{I'}_{|I_0^i}(\nabla^2 E\langle r^3 w_{IE}\rangle + \nabla^2 I\langle r^3 w_{II}\rangle)] \tag{26}$$

Equations 25 and 26 are of the reaction-diffusion type for the inhibitory and the excitatory fields in a two dimensional space. Defining $V(x,t) = \begin{pmatrix} E(x,t) \\ I(x.t) \end{pmatrix}$, D as the diffusion matrix and $f : R^2 \to R^2$ as the gain function, one can rewrite the above equations in the following form:

$$\tau\frac{\partial V(x,t)}{\partial t} = D\nabla^2 V(x,t) + f(V(x,t)) \tag{27}$$

The ODE part of this equation is the dynamic of a single EI population. The corresponding low firing fixed point (E_0, I_0) is stable in a specific parameter regime. It usually loses stability either via a saddle-node or a Hopf bifurcation which leads to either a region of bi-stability of low and high firing states or the emergence of oscillations. However, still far away from the bifurcation point since the diffusion matrix is not a scalar multiple of the identity, Turing instabilities can occur in the system. It means that the homogeneous state of $[E(x,t), I(x,t)] = [E_0, I_0]$ can become unstable. In other words, when the diffusion coefficients of the inhibition and the excitation are sufficiently different, the homogenous steady state becomes unstable because of the diffusion. To see this, noting that the above ODE has a homogeneous solution at $V_0 = [E_0, I_0]$, by linearization of the equation around the fixed point, i.e., $V(x,t) = V_0 + v(x,t)$, and plugging in the ansatz $v(x,t) = e^{ikx+\lambda(k)t}\psi$ we arrive at :

$$\begin{pmatrix} -D_{EE}K^2 + \partial_{E|V_0} f_E, -D_{EI}K^2 + \partial_{I|V_0} f_E \\ -D_{IE}K^2 + \partial_{E|V_0} f_I, -D_{II}K^2 + \partial_{I|V_0} f_I \end{pmatrix} \psi = \lambda\psi \tag{28}$$

Assume L to be the Jacobian of an isolated EI population rate equation at $K = 0$, then the condition for the stability of the fixed point reads as :

$$\begin{aligned} &\partial_E f_E + \partial_I f_I < 0 \\ &det(L) = \partial_E f_E \partial_I f_I - \partial_I f_E \partial_E f_I > 0 \end{aligned} \tag{29}$$

For the occurrence of a Turing instability at a critical k_c the eigenvalues $\lambda(k)$ which satisfy the characteristic equation below should become positive for some real value of k:

$$\lambda^2 + ((D_{EE} + D_{II})k^2 - (\partial_E f_E + \partial_I f_I)\lambda + R(k^2) = 0 \tag{30}$$

with $R(k^2)$ defined as

$$R(k^2) = \alpha k^4 - k^2(D_{EE}\partial_I f_I + D_{II}\partial_E f_E - D_{IE}\partial_I f_E - D_{EI}\partial_E f_I) + det(L) \tag{31}$$

in which $\alpha := D_{EE}D_{II} - D_{EI}D_{IE}$. Since the coefficient of λ in the equation (30), i.e., the negative sum of the eigenvalues, is positive, the necessary condition for the Turing instability is that $R(k^2) < 0$ for some k . When $\alpha > 0$, which is a reasonable assumption as the inhibitory connections are more local than the excitatory ones, if $\beta := D_{EE}\partial_I f_I + D_{II}\partial_E f_E - D_{IE}\partial_I f_E - D_{EI}\partial_E f_I > 0$ then $R(k^2)$ can become negative. In general $\frac{\beta}{\alpha}$ should be positive and instability of the homogenous state occurs at the value $k_0^2 = \frac{\beta}{2\alpha}$ for which $R(k)$ becomes zero for the first time. In the following, we consider the case of the local inhibitory connection and therefore, we take D_{II} and D_{EI} to be very small. Furthermore, we assume that we are in the regime of positive α, i.e., $D_{EE} > D_{IE}$ and $D_{II} \approx D_{EI} \ll D_{EE}$. With these assumptions, which are intuitively valid based on the connectivity structure in the cortex, the condition for positive β becomes:

$$D_{EE}\partial_I f_I - D_{IE}\partial_I f_E > 0 \tag{32}$$

This holds when D_{IE} and $\mid \partial_I f_E \mid$ are sufficiently large which means that the excess inhibition will produce a larger effect on the excitatory connection than the inhibitory one. This happens when the average stationary state potential distribution for neurons is close to the threshold, at which the effect of inhibition is larger than excitation. Therefore, conditions for a Turing instability to occur are:

$$\begin{aligned} &\mid \partial_I f_E \mid > \frac{D_{EE}}{D_{IE}} \mid \partial_I f_I \mid \\ &\mid \partial_I f_I \mid > \partial_E f_E \\ &\partial_E f_I > \frac{\partial_E f_E \mid \partial_I f_I \mid}{\mid \partial_I f_E \mid} \end{aligned} \tag{33}$$

Since $D_{EE}$and D_{IE} are proportional to W_{EE} and W_{IE} and the partial derivatives in the first approximations are equal to the average connection strength, the necessary conditions for the Turing instability reduce to

$$\begin{aligned} &W_{IE} \mid W_{EI} \mid > W_{EE} \mid W_{II} \mid \\ &W_{EE} - \mid W_{II} \mid < 0 \end{aligned} \tag{34}$$

As can be seen in Fig.1 and from the discussions following Eq(13), STDP leads to the regime where the above conditions are satisfied. Moreover, taking $\partial_E f_I \propto W_{IE}$ and ρ_{ext} as the free parameters, one can obtain the boundary of

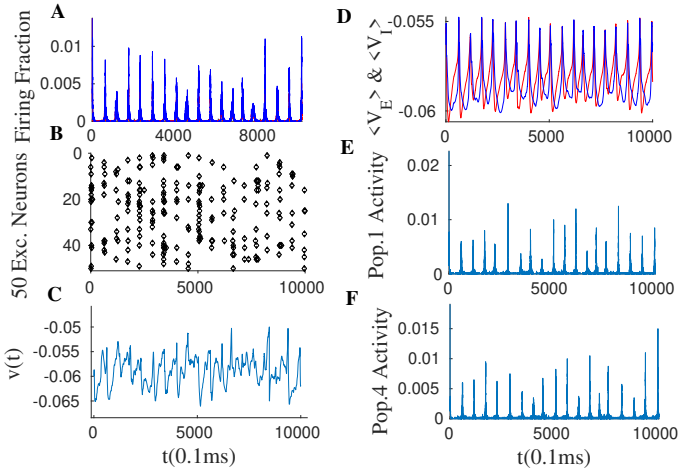

Fig. 9: Simulation result of 20 interconnected EI populations each of size $N_E = 10000$ arranged on a ring. Average synaptic weights between two different EI subnetworks decay with the phase difference of them. Parameters of synaptic weights in each EI population are $W_{EE} = 0.6$, $W_{EI} = 2, W_{II} = 2, W_{IE} = 0.75$,$\rho^E_{Ext} = 230Hz$ and $\rho^I_{Ext} = 150Hz$. (A) The average firing rate of the whole network. (B) Raster plot of the sub-population of 50 neurons in one single EI subnetwork. Although neurons fire at avalanche times, they don't fire in all of them, which leads to high variability in their interspike interval times. (C) The membrane potential of a single neuron, which is in a constant transition between a state close to the threshold and a state close to the resting potential. (D) The average membrane potential of an EI-population (red for Exc. and blue for Inh.). (E-F) The activity of two distinct EI subpopulations, showing high variability in sizes of avalanches in both of them.

the Turing instability region defined by $\min(R(k^2)) = 0$ at some value $k = k_c$. In this Turing instability region, stripe-like stationary patterns of activity with spatial frequencies close to $k = k_c$ appear in the system and the homogeneous solution becomes unstable. Besides Turing instabilities, it can also happen that the fixed point itself loses its stability at $k = 0$ through a Hopf bifurcation, where the real part of the eigenvalues of L becomes zero:

$$\begin{aligned} &\partial_E f_E + \partial_I f_I = 0 \\ &det(L) = \partial_E f_E \partial_I f_I - \partial_I f_E \partial_E f_I > 0 \end{aligned} \tag{35}$$

Furthermore, exactly at the BT point, we would also have $det(L) = 0$. Fig.9 shows the activity of 20 interconnected EI-populations each operating close to the BT point. Overall activity in this system is of synchronous avalanches type. Up-down state transitions also become synchronized. We can model weakly interconnected EI populations in the avalanche regime which shows oscillation

of frequency ω_i as pulse-coupled oscillators and therefore investigate conditions on synchronization and traveling wave solutions. This analysis is out of the scope of the current work. Another approach consists in supplementing the macroscopic field equation with an appropriate noise term to derive the mesoscopic equation. As can be seen from Fig.9, the overall network activity is of avalanche type. This provides again evidence that avalanches are scale-free and occur in different temporal and spatial scales. However, our neural field model still lacks the internal finite-size fluctuation effects, inhomogeneities, and cross-correlation between individual neurons, and also inter-populations correlations.

3.4 Stochastic neural field

3.4.1 Finite size fluctuations in a single EI population

So far we have analyzed mean-field models which were based on neglecting finite system size, inhomogeneities in the synaptic connections, and stochastic effects. Far from bifurcations of the mean-field (MF) equations, the behavior of the average rates of the stochastic system follows predictions of MF accurately. In this case, basins of attraction of the fixed points are separated enough and stochastic effects do not lead to a change in the macroscopic behavior of the system. However, close to the bifurcation points of the macroscopic system, internal and external fluctuations can cause the stochastic system to evolve differently from predictions of MF models. For example, it can cause transitions between different fixed points. Let us consider a homogeneous network of size N in which temporal and spatial variances in the firing rates of neurons are minimal. In this network, fluctuations in the finite system firing rates in the steady-state will be proportional to $O(\frac{1}{\sqrt{N}})$. To model the finite-size stochastic effects, we need to write down dynamics of micro-state evolution that match the mean-field upon coarse-graining. As we have seen, the operating region of the EI population is around a low firing state where neurons fire with high variability of inter-spike intervals indicating that we can model their spiking as a Poisson process. In this regime of activity, the Poisson neuron assumption enables us to write down the microscopic evolution of a model neuron with two active and inactive states. The transition rate α between the active and the inactive state should model vanishing of the postsynaptic potentiation, and the rate of inactive to active transition depends on the input and is therefore denoted by $f(i)$. We want to model the system in the statistical homogenous state, in which the probability that a neuron fires depends only on the number of active neurons and therefore is the same for every neuron in the population.

In the sequel, we consider a population of N_E excitatory and N_I inhibitory neurons, in which neurons change their states independently. Let us take $P(E, I, t)$ as the probability density of the EI population being in a state with E the number of active excitatory and I the number of active inhibitory neurons at time t. The following master equation describes the microscopic

evolution of the system:

$$\begin{aligned}\frac{\partial P(E,I,t)}{\partial t} =& -\alpha[(EP(E,I,t)+IP(E,I,t)] \\ &+\alpha[(E+1)P(E+1,I,t)+(I+1)P(E,I+1,t)] \\ &+(N_E-E+1)f(c_{EE}(E-1),c_{EI}I)P(E-1,I,t) \\ &-(N_E-E)f(c_{EE}E,c_{EI}I)P(E,I,t) \\ &+(N_I-I+1)g(c_{IE}E,c_{II}(I-1))P(E-1,I,t) \\ &-(N_I-I)g(c_{IE}E,c_{II}I)P(E,I,t) \end{aligned} \tag{36}$$

in which $c_{xy}=\frac{K_{xy}}{N_x}w_{xy}$, with K_{xy} being the number of incoming connections to a neuron in the population x from the population y , $f(.)$ and $g(.)$ are rates of inactive to active transtition for excitatory and inhibitory neurons,respectively. We use the system size expansion method Van kampen (2007) for truncating the moment hierarchy based on taking an ansatz on the order of the finite size fluctuation in the system. Assuming fluctuations around the deterministic (average field) trajectory to be of order $O(N)$, we can rewrite our stochastic variables in terms of a deterministic and a fluctuating term as

$$E=N_E\rho_E+N_E^{1/2}\epsilon, \qquad I=N_I\rho_I+N_I^{1/2}i \tag{37}$$

where ϵ and i are representing fluctuations around the deterministic trajectories. Defining $P(E,I,t)=Q(\epsilon,i,t)$, we can rewrite the l.h.s. of the master equation in terms of the new parameters as

$$\frac{\partial P(E,I,t)}{\partial t}=\frac{\partial(\epsilon,i,t)}{\partial t}-N_E^{1/2}\frac{d\rho_E(t)}{dt}\frac{\partial Q}{\partial\epsilon}-N_I^{1/2}\frac{d\rho_I(t)}{dt}\frac{\partial Q}{\partial i} \tag{38}$$

Defining ladder operators $Z_Ef(E)=f(E+1)$ and $Z_E^{-1}f(E)=f(E-1)$ and expanding them in powers of ϵ , we arrive :

$$\begin{aligned}Z_E &= 1+N_E^{-1/2}\frac{\partial}{\partial\epsilon}+\frac{1}{2}N_E^{-1}\frac{\partial^2}{\partial^2\epsilon}+... \\ Z_E^{-1} &= 1-N_E^{-1/2}\frac{\partial}{\partial\epsilon}+\frac{1}{2}N_E^{-1}\frac{\partial^2}{\partial^2\epsilon}+... \end{aligned} \tag{39}$$

We define the same ladder operators for the inhibitory population states. Plugging all these equations into the master equation (36), we have:

$$\begin{aligned}&\frac{\partial Q(\epsilon,i,t)}{\partial t}-N_E^{1/2}\frac{d\rho_E(t)}{dt}\frac{\partial Q}{\partial\epsilon}-N_I^{1/2}\frac{d\rho_I(t)}{dt}\frac{\partial Q}{\partial i}=\alpha(Z_E-1)[(N_E\rho_E+N_E^{1/2})\epsilon)Q] \\ &+(Z_E^{-1}-1)[N_E(1-\rho_E-N_E^{-1/2}\epsilon)*f(c_{EE}N_E(\rho_E+N_E^{-1/2}\epsilon),c_{EI}N_I(\rho_I+N_I^{-1/2}i))Q] \\ &+\alpha(Z_I-1)[(N_I\rho_I+N_I^{1/2}i)Q(\epsilon,i,t)]\end{aligned}$$

$$+ (Z_I^{-1} - 1)[N_I(1 - \rho_I - N_I^{-1/2} i) * g(c_{IE} N_E(\rho_E + N_E^{-1/2}\epsilon), c_{II} N_I(\rho_I + N_I^{-1/2} i))Q] \tag{40}$$

Expanding the inactive to active transition rates as

$$\begin{aligned} f(c_{EE} N_E(\rho_E + N_E^{-1/2}\epsilon), c_{EI} N_I(\rho_I + N_I^{-1/2} i)) =& f(c_{EE} N_E \rho_E, c_{EI} N_I \rho_I) \\ &+ N_E^{-1/2} \frac{\partial f}{\partial \rho_E}\epsilon + N_I^{-1/2} \frac{\partial f}{\partial \rho_I} i + ... \end{aligned} \tag{41}$$

Using the same expansion for ladder operators, we can sort the right and the left sides of equation (40) in powers of N_E and N_I . Equating terms of the order $O(N_E^{1/2})$ and $O(N_I^{1/2})$ leads to the macroscopic equation:

$$\begin{aligned} -\frac{d\rho_E(t)}{dt} &= \alpha\rho_E(t) - (1 - \rho_E(t)) f(\kappa_{EE} w_{EE} N_E \rho_E, \kappa_{EI} w_{EI} \rho_I) \\ -\frac{d\rho_I(t)}{dt} &= \alpha\rho_I(t) - (1 - \rho_I(t)) g(\kappa_{IE} w_{IE} N_I \rho_I, \kappa_{II} w_{II} \rho_I) \end{aligned} \tag{42}$$

Equating terms of order $O(N^0)$ leads to a linear FPE for $Q(\epsilon, i, t)$ of the form:

$$\begin{aligned} \frac{\partial Q(\epsilon, i, t)}{\partial t} =& (\alpha - (1 - \rho_E)\frac{\partial f}{\partial \rho_E} + f)\frac{\partial}{\partial \epsilon}\epsilon Q + (\alpha - (1 - \rho_I)\frac{\partial g}{\partial \rho_I} + f)\frac{\partial}{\partial i} i Q \\ &- (1 - \rho_E)\frac{\partial f}{\partial \rho_I}\frac{\partial}{\partial \epsilon} i Q - (1 - \rho_I)\frac{\partial g}{\partial \rho_E}\frac{\partial}{\partial i}\epsilon Q \\ &+ \frac{1}{2}(1 - \rho_E) f \frac{\partial^2}{\partial \epsilon^2} Q + \frac{1}{2}(1 - \rho_I) g \frac{\partial^2}{\partial i^2} Q \end{aligned} \tag{43}$$

Defining matrices A and B as

$$\begin{aligned} \begin{pmatrix} A_{11} & A_{12} \\ A_{21} & A_{22} \end{pmatrix} &= \begin{pmatrix} -\alpha + (1 - \rho_E)\frac{\partial f}{\partial \rho_E} - f & (1 - \rho_E)\frac{\partial f}{\partial \rho_I} \\ (1 - \rho_I)\frac{\partial g}{\partial \rho_E} & -\alpha + (1 - \rho_I)\frac{\partial g}{\partial \rho_I} - g \end{pmatrix} \\ B &= \begin{pmatrix} (1 - \rho_E) f & 0 \\ 0 & (1 - \rho_I) g \end{pmatrix} \end{aligned} \tag{44}$$

the amplitude of fluctuating term evolves as

$$\frac{\partial}{\partial t}\begin{pmatrix} \langle\epsilon\rangle \\ \langle i\rangle \end{pmatrix} = \begin{pmatrix} A_{11} & A_{12} \\ A_{21} & A_{22} \end{pmatrix}\begin{pmatrix} \langle\epsilon\rangle \\ \langle i\rangle \end{pmatrix} \tag{45}$$

The covariance matrix $C = \begin{pmatrix} Var(\epsilon) & Cov(\epsilon, i) \\ Cov(\epsilon, i) & Var(i) \end{pmatrix}$ satisfies :

$$\frac{\partial}{\partial t} C = AC + CA^t + B \tag{46}$$

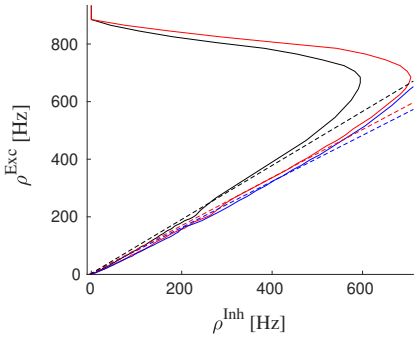

Fig. 10: Nullcline graphs for the system with parameters: $W_{EI} = 1.5, W_{II} = 2, W_{IE} = 0.75$, $\rho^I_{Ext} = 150Hz, \rho^E_{Ext} = 280Hz$,$w_{EE} = 0.53$(red) and 0.48(black). The blue curve is the inhibitory nullcline and dashed lines are linear approximations of the corresponding nullclines. Both excitatory nullclines have intersection with the inhibitory nullcline in the semi-linear section.

If the determinant of A is positive and its trace is negative at the stationary point of the macroscopic equation (i.e., A has two negative eigenvalues), then the averages of the fluctuation terms go to zero. At the stationary point of the macroscopic equation, we have:

$$\begin{pmatrix} A_{11} & 0 & A_{12} \\ 0 & A_{22} & A_{21} \\ A_{21} & A_{12} & A_{11}+A_{22} \end{pmatrix} \begin{pmatrix} Var(\epsilon)_{st} \\ Var(i)_{st} \\ Cov(\epsilon,i)_{st} \end{pmatrix} = -\frac{\alpha}{2} \begin{pmatrix} \rho^{st}_E \\ \rho^{st}_I \\ 0 \end{pmatrix} \tag{47}$$

which has the solution :

$$\begin{aligned} Var(\epsilon)_{st} &\approx c((A_{11}A_{22} - A_{21}A_{12} + A^2_{22})\rho_E + A^2_{12}\rho_I) \\ Var(i)_{st} &\approx c((A_{11}A_{22} - A_{21}A_{12} + A^2_{11})\rho_I + A^2_{21}\rho_E) \\ Cov(\epsilon,i)_{st} &\approx -c(A_{11}A_{12}\rho_I + A_{21}A_{22}\rho_E) \end{aligned} \tag{48}$$

with $c = \dfrac{-\alpha}{2(A_{11}+A_{22})(A_{11}A_{22} - A_{21}A_{12})}$.

The average population rate and the fluctuation arround the macroscopic state are:

$$\begin{aligned} \langle \frac{E}{N_E} \rangle &= \rho_E \qquad Var(\frac{E}{N_E}) = \frac{Var(\epsilon)}{N_E} \\ \langle \frac{I}{N_I} \rangle &= \rho_I \qquad Var(\frac{I}{N_I}) = \frac{Var(i)}{N_I} \end{aligned} \tag{49}$$

From equations (48) and (49), it can be seen that close to the bifurcation of the macroscopic equation, i.e., the BT point, where both trace and determinant of the Jacobian are close to zero, fluctuation magnitudes increase. Exactly at the bifurcation point, the mentioned system size expansion fails because the average of the noise term is unbounded, and therefore, we cannot assume the fluctuating term in equation (37) to be of order $N^{1/2}$. Figures (11-13) show characteristics of an EI population activity in the Poisson regime. Fig.10 is the nullcline graph related to two different strengths of W_{EE} both of them adjusting the system to have a stable fixed point on the semi-linear part of the nullclines. The one with a higher W_{EE} has a higher firing rate fixed point. Fig.11 shows how the average and the variance of the membrane potential, the average rates, and the inter-spike interval CV follow the prediction that neurons fire with Poisson statistics, asynchronously and independently. The dashed lines in Fig.11 show the approximation with neurons firing with Poisson statistics and independently with the same rates that we observe in the simulation of the network. The dashed lines in the bottom-left plot show the rate approximation with the membrane potential distribution being Gaussian with the mean and the variance as predicted in the top panel. Fig.12A shows that the variance and the covariance of the excitatory and the inhibitory rates in the simulation match the values derived from the microscopic model discussed above, i.e., equations (48) and (49).

3.4.2 Stochastic neural field with a tuning mechanism to the critical state

We have considered the situation where the inhibition effect in the network is local and we have seen that the system is tuned in a way that the inhibitory feedback in the local EI population balances the average excitatory current in a way that neuronal firing is fluctuation driven. If the effect of the inhibitory current is instantaneous, we can use proportionality of excitatory and inhibitory currents to write down rate dynamics of the excitatory population in terms of a stochastic field equation when both inhibitory feedback and fluctuations are local. From equation (14), we know that near the BT point, there is a linear relation between rates, i.e., $I \approx \frac{c_{EE}}{c_{EI}} E$. Therefore, the average current to the excitatory population close to the BT point (Eq.6) can be written as $\gamma = c_{EE}E - c_{EI}I \approx 0$. The second derivative in the expansion of the gain function for the excitatory population from equation (27) in the region of low activity is

$$\frac{1}{2}\frac{\partial^2 f}{\partial E^2}E^2 + \frac{\partial^2 f}{\partial EI}EI + \frac{1}{2}\frac{\partial^2 f}{\partial I^2}I^2 \tag{50}$$

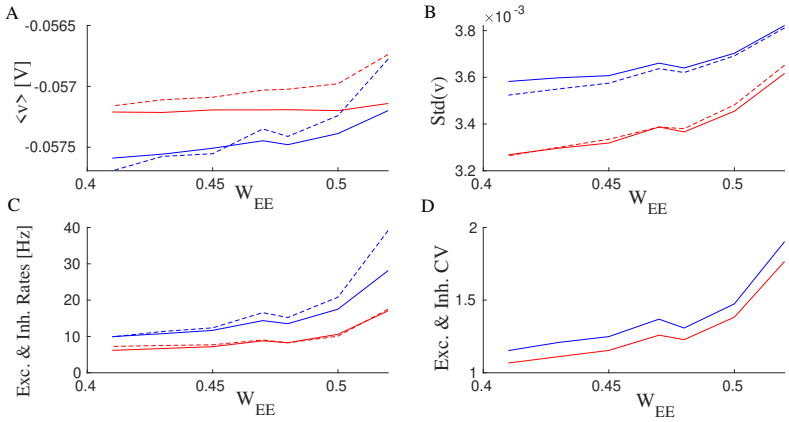

Fig. 11: Characteristics of the network activity for systems with $W_{EI} = 1.5, W_{II} = 2, W_{IE} = 0.75$, $\rho^I_{Ext} = 180Hz, \rho^E_{Ext} = 300Hz$ and $W_{EE} \in [0.41, 52]$ which shows near Poisson firing and avalanche dynamics in smaller values of W_{EE} in the mentioned value range. Red curves show excitatory quantities and blue is for inhibitory ones. Dashed lines are the prediction from the Poisson assumption and solid lines are the simulation results. (A) Average membrane potential. (B) The standard deviation of the membrane potential. (C) Output rates. Here, dashed lines are the firing rates derived from the Gaussian approximation of the potential distribution based on values of the average and the variance of the membrane potential in the top panel of this figure. (D) CV of interspike intervals in the simulation.

where we can use the following approximations for the gain function derivatives:

$$\frac{\partial^2 f}{\partial I^2} \propto W_{EI}^2, \quad \frac{\partial^2 f}{\partial E^2} \propto W_{EE}^2, \quad \frac{\partial f}{\partial I \partial E} \propto -W_{EE} W_{EI} \tag{51}$$

By using the linear relation of the inhibitory and excitatory rates near the BT as the result of the projection of the dynamic to the slow manifold, we can replace inhibitory local field strength by a term linear in the local excitatory field. Besides, fluctuations in the average population activity, Eq.(49), linearly depend on the rate. Therefore, we can write down the stochastic field equation for the excitatory rate in the region of small γ:

$$\begin{aligned} &\frac{\partial E(x,t)}{\partial t} = \gamma E(x,t) + D\Delta E(x,t) - \mathsf{u}E^2(x,t) + \psi(x,t) \\ &\langle \psi(x,t)\psi(x',t') \rangle = 2\sqrt{\frac{\sigma^2}{N}} E(x,t)\delta(x-x')\delta(t-t') \end{aligned} \tag{52}$$

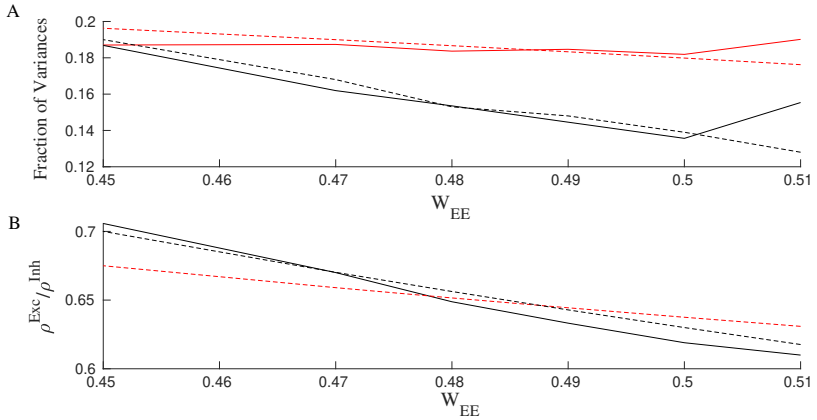

Fig. 12: (A) Ratio of var(E) to var(I) (red) and var(EI) to var(I)(black) in the stationary state of the above mentioned systems. Dashed lines are the approximation derived from the Poisson assumption and solid lines are the simulation results of the spiking neuron network. (B) The ratio of the excitatory to the inhibitory stationary rates varies vs. W_{EE}. The dashed line is $\frac{k_{EI}W_{EI}}{k_{EE}W_{EE}}$ and the solid line is the simulation result.

Here $u < 0$ is the coefficient related to synaptic weights that can be explicitly derived by assuming a certain form of the gain function and proportionality of the rates. This stochastic partial differential equation after appropriate rescaling $E(x,t) = \frac{\sigma}{u\tau} S(x,t)$ agrees with the Langevin description of directed percolation which is of the following form with new transformed coefficients :

$$\frac{\partial S(x,t)}{\partial t} = (\gamma' + D'\Delta)S(x,t) - u'S^2(x,t) + \psi(x,t)$$
$$\langle \psi(x,t)\psi(x',t')\rangle = 2u'S(x,t)\delta(x-x')\delta(t-t') \tag{53}$$

At $\gamma' = 0$, the above system shows an absorbing state phase transition. Thus, from any active state the system relaxes by avalanches with a power-law size distribution to an inactive state.

In an isolated EI population, external drive to the inhibitory and the excitatory population should be present to counterbalance the dissipation by the leaking currents and to thereby set the average membrane potential in these neurons at a state above the resting threshold. External excitatory input to the excitatory population is slightly higher than the external drive to the inhibitory population which leads to a slightly higher average membrane potential in the excitatory population. Furthermore, we can assume that the external spike train to each neuron is Poisson as well. The external drive by itself would not lead to significant firing in the individual neurons but the strengths of the internal connections between them are tuned in a way that bursts of activity

occur in the excitatory population which is then followed by the inhibitory ones. The internal feedback inhibition is strong enough to kill the excitatory burst. In a slightly inhibition-dominated regime, we have sharp synchronous responses to the external input in a short time window. On the other hand, the network has a safe margin from an overly active state. In the absence of the input distinguished from random external noise, the system shows scale-free avalanches because of the maintenance of the inhibition-excitation balance. However, the external drive must compensate for the dissipation for the system tostay at or near the critical point. Without mechanisms like short-term plasticity, the external drive has be fine-tuned for the system to show criticality. However, short-term plasticity in a network in which synaptic weights are already near a slightly inhibition dominated regime broadens the range of the external drive strength which leads to critical avalanches. We can extend the short term synaptic depression of equation(8) to a continuum field equation by defining a field of excitatory synaptic efficacy $\Omega(x,t) \propto \langle W_{EE} \rangle(x,t)$ with local dynamics of equation (16):

$$\begin{aligned}
\tau_m \frac{\partial E(x,t)}{\partial t} &= (-\alpha + \Omega(x,t))E(x,t) + D\Delta E(x,t) - \mathsf{u}E^2(x,t) + \psi(x,t) \\
\frac{\partial \Omega(x,t)}{dt} &= \frac{1}{\tau_{STP}}(\Omega_0 - \Omega) - q\Omega E(x,t) \\
\langle \psi(x,t)\psi(x',t') \rangle &= 2\sqrt{\frac{\sigma^2}{N}} E(x,t)\delta(x-x')\delta(t-t')
\end{aligned} \tag{54}$$

Here α represents both the decay of activity by leaky currents of the cells and the inhibition feedback which varies linearly with the excitatory rate. The dynamic excitatory synaptic strength brings the coefficient of the linear term to a value near zero (see Fig.13). This set of equations has a stationary synaptic efficacy solution of the value

$$\Omega_{st} = \frac{\Omega_0}{1 + q\tau_{STP}E_{st}} \tag{55}$$

On the other hand in the active phase, the stationary homogeneous rate is :

$$E_{st} = \frac{-\alpha + \Omega_{st}}{\mathsf{u}} \tag{56}$$

Assuming u is a very small quantity and E_{st} is also small in the low firing rate regime then $-\alpha + \Omega_{st} \approx 0$ and $E_{st} = \frac{1}{q\tau_{STP}}(\frac{\Omega_0}{\alpha} - 1)$.

Long-term synaptic plasticity tunes Ω_0 so that the coefficient of the linear term is close to zero and a moderate level of short-term depression suffices to bring the system to the critical point. Altogether, equation (54) is the description of an EI interconnected spiking neuron network tuned to the critical point of balancing inhibition and excitation both by long-term synaptic plasticity

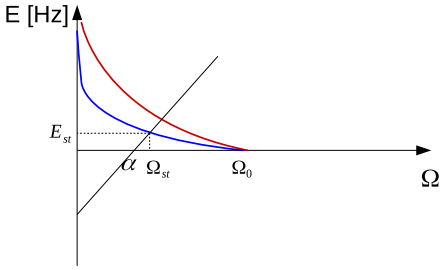

Fig. 13: Intersection of curves given by equations (55) and (56). Setting Ω_0 to a value close to α by STDP and sufficient amount of synaptic depression leads to a stationary value of Ω_{st} very close to the critical value. The blue curve is associated to a higher value of q.

and short-term synaptic depression. The system wanders around the phase transition point and shows avalanche dynamics with scale-free size and time distribution, the proportionality of inhibition and excitation, up and down state transitions of the membrane potential and population activity rates, and oscillations of order of $10Hz$ resembling ubiquitous alpha-band oscillations.

4 Discussion

In this work, we have proposed a self-organizing model for the cortical dynamics which tunes the system to the regime of low firing avalanche dynamics corresponding to the ongoing intrinsic activity in the cortex. We showed that long-term synaptic plasticity by STDP tunes the synaptic weights to achieve the internal balance of inhibition and excitation. This effect does not depend on the exact shape of STDP kernels. On the other hand, short-term synaptic depression can tune the system in response to the wide range of the strength of the external drive.

In the vicinity of the bifurcation point, fluctuation effects are manifested strongly and mean-field solutions do not adequately describe the dynamics. In particular, internal and external noises which were neglected in the mean-field analysis can induce state transitions in the proximity of the saddle-node line. On the other hand, in the vicinity of the Hopf bifurcation line, fluctuations lead to higher variability in the amplitude of avalanches. In the vicinity of the BT point, by analyzing the linear stability of the quiescent fixed point, slow dynamics can be projected to the nonlinear stable manifold. We wrote down dynamics in terms of the excitatory field only assuming a fast linear inhibitory feedback. The dynamical equation for the excitatory field matches the description of directed percolation. At the balance line, the coefficient of the linear term in the field equation vanishes which puts the system at the critical point of the percolation phase transition. Modeling the whole dynamic as a directed percolation of two dynamical variables is another possibility that we have not explored.

In an open system, the external load has to be fine-tuned to compensate for the dissipation in order to remain at the critical point. Short-term depression of excitatory synapses allows this tuning for a wider range of external drives. We have not considered short-term plasticity for other types of synapses. However, we believe that under appropriate conditions on their respective strengths, we can observe the same qualitative regulation effects.

Conflict of Interest Statement

The authors declare that the research was conducted in the absence of any commercial or financial relationships that could be construed as a potential conflict of interest.

Author Contributions

M.E. and J.J. designed research. M.E. performed research. M.E. wrote the manuscript. J.J. edited the manuscript. All authors reviewed the manuscript, contributed to the article, and approved the submitted version.

Funding

This study was funded by the International Max Planck Reseach School and the Max Planck Institute for Mathematics in Sciences in Leipzig.

Acknowledgments

Open access funding provided by Max Planck Society. ME wants to thank International Max Planck Reseach School for funding his position during the research period.

Data Availability Statement

The original contributions presented in the study are included in the article/-supplementary material, further inquiries can be directed to the corresponding author.

References

Amari S (1977) Dynamics of pattern formation in lateral-inhibition type neural fields. Biol Cybern 27, 77–87 https://doiorg/101007/BF00337259

Beggs J, Plenz D (2003) Neuronal avalanches in neocortical circuits. Journal of Neuroscience,23 (35) 11167-11177; DOI: 101523/JNEUROSCI23-35-111672003

Benayoun M, Cowan J, van Drongelen W, et al (2010) Avalanches in a stochastic model of spiking neurons. PLoS Comput Biol 6(7): e1000846 DOI:101371/journalpcbi1000846

Bornholdt S, Roehl T (2003) Self-organized critical neural networks. Phys Rev E 67, 066118 DOI:101103/PhysRevE67066118

Bressloff P (2000) Stochastic neural field theory and the system-size expansion. SIAM J Appl Math Vol 70, Iss DOI: 5101137/090756971

Bressloff P (2011) Spatiotemporal dynamics of continuum neural fields. Journal of Physics A: Mathematical and Theoretical Volume 45, Issue 3, article id 033001, 109 pp DOI: 101088/1751-8113/45/3/033001

Bressloff P (2019) Stochastic neural field model of stimulus-dependent variability in cortical neurons. PLoS computational biology vol 15,3 e1006755DOI:101371/journalpcbi1006755

Brochini L, de Andrade Costa A, Abadi M, et al (2016) Phase transitions and self-organized criticality in networks of stochastic spiking neurons. Sci Rep 6, 35831 DOI: 101038/srep35831

Brunel N (2000) Dynamics of sparsely connected networks of excitatory and inhibitory spiking neurons. J Comput Neurosci 8, 183–208 (2000) https://doiorg/101023/A:1008925309027

Brunel N, Hakim V (1999) Fast global oscillations in networks of integrate-and-fire neurons with low firing rates. Neural Comput 1999 Oct 1;11(7):1621-71 doi: 101162/089976699300016179 PMID: 10490941

Brunel N, Hakim V (2008) Sparsely synchronized neuronal oscillations. Chaos 18, 015113 (2008); https://doiorg/101063/12779858

Buice M, Cowan J (2007) Field-theoretic approach to fluctuation effects in neural networks. Phys Rev E 75, 051919 DOI:101103/PhysRevE75051919

Burkitt A, Gilson M, van Hemmen J (2007) Spike-timing-dependent plasticity for neurons with recurrent connections. Biol Cybern 96(5):533-46 doi: 101007/s00422-007-0148-2 Epub 2007 Apr 6 PMID: 17415586

Chialvo D (2004) Critical brain networks. Journal Physica A: Statistical Mechanics and its Applications,Volume 340, Issue 4, 15 September 2004, Pages 756-765, DOI:101016/jphysa200405064

Chialvo D (2010) Emergent complex neural dynamics. Nature Phys 6, 744–750 (2010) https://doiorg/101038/nphys1803

Cowan D, Neuman J, Kiewiet B, et al (2013) Self-organized criticality in a network of interacting neurons. J Stat Mech P04030 DOI:101088/1742-5468/2013/04/P04030

Câteau H, Fukai T (2003) A stochastic method to predict the consequence of arbitrary forms of spike-timing-dependent plasticity. A Neural Comput 15(3):597-620 doi: 101162/089976603321192095 PMID: 12620159

Doi M (1976) Second quantization representation for classical many-particle systems. J Phys A: Math Gen 9 1465

Ehsani M, Jost J (2022) Scale-free avalanches in excitatory-inhibitory populations of spiking neurons with conductance based synaptic currents[preprint]. http://arxivorg/abs/220307834

Ermentrout B (1998) Neural networks as spatio-temporal pattern-forming systems. Rep Prog Phys 61 353

Ermentrout G, Cowan D (1979) A mathematical theory of visual hallucination patterns. Biol Cybernetics 34, 137–150 https://doiorg/101007/BF00336965

Gerstner W, Kempter R, van Hemmen J, et al (1996) A neuronal learning rule for sub-millisecond temporal coding. Nature 383, 76–78 DOI: 101038/383076a0

Ginzburg I, Sompolinsky H (1994) Theory of correlations in stochastic neural networks. Phys Rev E Vol50 https://doiorg/101103/PhysRevE503171

Hahn G, Petermann D, Havenith M, et al (2010) Neuronal avalanches in spontaneous activity in vivo. J Neurophysiol Volume 104 Issue 6 ,3312-3322DOI:101152/jn009532009

Hardstone R, Poil S, Schiavone G, et al (2012) Detrended fluctuation analysis: a scale-free view on neuronal oscillations. Front Physio 3:450 doi: 103389/fphys201200450

Kempter R, Gerstner W, van Hemmen J (2001) Intrinsic stabilization of output rates by spike-based hebbian learning. Neural Comput(12):2709-41 doi: 101162/089976601317098501 PMID: 11705408

Kistler W, van Hemmen J (1999) Short-term synaptic plasticity and network behavior. Neural Comput11(7):1579-94 doi: 101162/089976699300016151 PMID: 10490939

Kistler W, van Hemmen J (2000) Modeling synaptic plasticity in conjuction with the timing of pre- and postsynaptic action potentials. Neural Comput 12(2):385-405 doi: 101162/089976600300015844 PMID: 10636948

Levina A, Herrmann M, Geisel T (2007) Dynamical synapses causing self-organized criticality in neural networks. Nature Phys 3, 857–860 DOI:101038/nphys758

Levina A, Herrmann M, Geisel T (2009) Phase transitions towards criticality in a neural system with adaptive interactions. Phys Rev Lett 102, 118110 DOI:101103/PhysRevLett102118110

Linkenkaer-Hansen k, Nikouline V, Palva V, et al (2001) Long-range temporal correlations and scaling behavior in human brain oscillations. Journal of Neuroscience,21,1370-1377 https://doi.org/10.1523/JNEUROSCI.21-04-01370.2001

Meisel C, Gross T (2009) Adaptive self-organization in a realistic neural network model. Physical Review E80, 061917 DOI: 101103/PhysRevE80061917

Meyer C, van Vreeswijk C (2002) Temporal correlations in stochastic networks of spiking neurons. Neural Comput 369-404 DOI: 101162/08997660252741167 PMID: 11802917

Miller K, Sorensen L, G. O, et al (2009) Power-law scaling in the brain surface electric potential. PLoS computational Biology 5(12): e1000609 DOI:101371/journalpcbi1000609

Peliti L (1985) Path integral approach to birth-death processes on a lattice. Journal de Physique, 46 (9), pp1469-1483 DOI:ff101051/jphys:019850046090146900ff ffjpa-00210092f

Peng J, J. B (2013) Attaining and maintaining criticality in a neuronal network model. Physica A: Statistical Mechanics and its Applications Volume 392, Issue 7, 1611-1620 DOI: 101016/jphysa201211013

Petermann T, Thiagarajan T, Lebedev M, et al (2009) Spontaneous cortical activity in awake monkeys composed of neuronal avalanches. PNAS 106 (37) 15921-15926 DOI:101073/pnas0904089106

Pinto D, Ermentrout G (2001a) Spatially structured activity in synaptically coupled neuronal networks:lateral inhibition and standing pulses. SIAM J Appl Math Vol 62, Iss110 DOI: 1137/S0036139900346453

Pinto D, Ermentrout G (2001b) Spatially structured activity in synaptically coupled neuronal networks:traveling fronts and pulses. SIAM Journal on Applied Mathematics 62, no 1: 206–25 http://wwwjstororg/stable/3061903

Ribeiro T, Copelli M, Caixeta F, et al (2010) Spike avalanches exhibit universal dynamics across the sleep-wake cycle. PLoS ONE 5(11): e14129 https://doiorg/101371/journalpone0014129

van Rossum M, Bi G, Turrigiano G (2000) Stable hebbian learning from spike timing-dependent plasticity. Journal of Neuroscience 20 (23) 8812-8821; DOI: 101523/JNEUROSCI20-23-088122000

Rybarsch M, Bornholdt S (2014) Avalanches in self-organized critical neural networks: A minimal model for the neural soc universality class. PLoS ONE 9(4): e93090 DOI: 101371/journalpone0093090

di Santo S, Villegas P, Burioni R, et al (2018) Landau–ginzburg theory of cortex dynamics: Scale-free avalanches emerge at the edge of synchronization. PNAS 115 (7) E1356-E1365 DOI: 101073/pnas1712989115

Soula H, Chow C (2007) Stochastic dynamics of a finite-size spiking neural network. Neural Comput 19, 3262-92 DOI: 101162/neco200719123262 PMID: 17970653

Tagliazucchi E, Chialvo D (2013) Brain complexity born out of criticality. AIP Conference Proceedings 1510, 4 (2013); DOI:101063/14776495

Touboul J, Hermann G, Faugeras O (2015) Noise-indused behaviours in neural mean field dynamics. SIAM Journal on Applied Dynamical Systems Vol 11, Iss 110 DOI: 1137/110832392

Troy W, Shusterman V (2007) Patterns and features of families of traveling waves in large-scale neuronal. SIAM Journal on Applied Dynamical Systems 6(1):263-292 DOI:101137/06066638X

Tsodyks M, Markram H (1997) The neural code between neocortical pyramidal neurons depends on neurotransmitter release probability. Proc Natl Acad Sci USA Jan 21;94(2):719-23 DOI: 101073/pnas942719

Van kampen N (2007) Stochastic Processes in Physics and Chemistry. volume in North-Holland Personal Library Book

Wilson H, Cowan J (1972) Excitatory and inhibitory interactions in localized populations of model neurons. Biophys J 1972;12(1):1-24 doi:101016/S0006-3495(72)86068-5

Wilson H, Cowan J (1973) A mathematical theory of the functional dynamics of cortical and thalamic nervous tissue. Kybernetik 13, 55–80 https://doiorg/101007/BF00288786